DIRECT MEASUREMENT OF SOLID DRAG FORCE IN FLUID–PARTICLE FLOW

ANA MOSQUERA GOMEZ, MARKKU NIKKU & PAYMAN JALALI
LUT Energy, Lappeenranta University of Technology, Finland

ABSTRACT
Many industrial applications involve fluidization systems in which it is possible to distinguish solid particles acting as a separate phase. The fluid–particle drag forces are well known and have been widely described in the literature to account for the momentum transfer between the phases whereas the study of particle–particle interaction still has several challenges especially for dense flow regimes. In this work, a novel method for the measurement of the particle–particle drag force was developed, using a cantilever beam with four strain gauges. For validation purposes, fluid–particle drag was investigated, the measurement device was evaluated considering two systems, in the first case, a spherical object was exposed to an air flow in a vertical tube where different velocities were used and for the second one, the forces resulting from impinging jet flows on the sphere were considered. The results show good agreement with the theoretical values. The results show good agreement with the theoretical values. The average magnitude of drag force upon a larger spherical object immersed on a flow of small particles was measured under different streams conditions, for different impinging height, size, and density of the particles.
Keywords: particle–particle drag force, fluid–particle drag force, strain gauge, impinging jet.

1 INTRODUCTION
Fluidized bed processes are utilized in a variety of industrial applications due to their high heat and mass transfer rates between the fluid and solid phase. For many decades, significant effort has been dedicated to increasing the understanding of the multiphase flow in these fluid–particle systems to improve on the design and scale-up of fluidized beds. The advances in computational performance have increased the popularity of numerical modelling in studies of fluidized beds, but due to the complexity of the fluid–particle and particle–particle interactions, active research is ongoing in this area.

Two approaches can be utilized in simulations of fluid–particle flows, an Eulerian–Lagrangian formulation, which treats the particles as a discrete phase and the fluid as a continuous phase, or an Eulerian–Eulerian approach, where both phases are considered continuous. Both approaches have their advantages and disadvantages, namely the Eulerian–Lagrangian approach can be computationally more expensive when the number of particles increases, though this can be somewhat remedied with grouping methods such as multiphase particle-in-cell method. For many large scale fluidized beds, the Eulerian–Eulerian approach is still more practical.

The description of particle as a continuous phase is based on the Kinetic Theory of Granular Flows [1], [2], which makes simplifications and models all the particle level phenomena, such as the particle collisions. For high solids concentrations, the collisional and frictional interactions between the particles increases and their effect is significant on the system behaviour, and in these conditions, the Eulerian models may fail to correctly predict the particle interactions [3]. As the Eulerian approach cannot consider momentum transfer and movements of individual particles, the momentum transfer is modelled as a drag force similarly to fluid–solid momentum transfer.

Literature presents several studies for fluid–particle drag force but for particle–particle drag force only a few studies can be found [4], [5]. These models are developed for or assume

that all the particles are monosized spheres, and in the Eulerian approach the particle are distributed uniformly inside every computational cell. Both assumptions may affect the model results, especially when the size ratio between the particles is large.

Measuring the collisional force between two individual particles is possible but when the number of particles and collisions increase, is not any more feasible. In the present study, collisional forces from falling particles are measured using a force sensor based on strain gauges. The aim of the method is to be able to measure the net momentum transfer from the collisions, i.e. the drag force from the particle phase, in real process conditions, for example inside fluidized beds, to enable particle–particle drag force model development. Strain gauge systems have been previously used for direct measurement of forces and moments [6], [7]. The measurement method, sensor layout and calibration are explained in the next section. The validation measurements of fluid–particle drag force and experimental results of particle forces generated by a cloud of particles colliding with a large sphere are presented and discussed in Section 3. Finally, the concluding remarks and application perspective of the developed force measurement system are presented in Section 4.

2 FORCE SENSOR DEVELOPMENT AND CALIBRATION

When strain gauges pairs are arranged in a Wheatstone bridge circuit, the electric resistance of them can be affected by external forces and the output voltage reading is directly related to those applied forces. Four strain gauges (Kyowa KFG-1b-120-c1) were mounted on a rectangular steel beam (SAE 1074, 3 mm x 0.5 mm) to measure bending moment applied to the beam, and a spherical plastic particle of 40 mm diameter (table tennis ball) was attached to the tip of the steel beam. The elasticity modulus of the used steel was $2.10 \cdot 10^9$ N/m^2. The other end of the beam was fixed with a rigid support. A full Wheatstone bridge was used to increase the sensitivity and signal to noise ratio of the measurement signal. The sensor was connected to an analog data acquisition board and data were recorded at a frequency of 200 Hz using LabVIEW and processed with a low-pass filter. The sensor was calibrated with a set of known weights in order to correlate the voltage signal of the sensor to known gravitational forces. A schematic of the measurement system and the calibration curve are presented in Fig. 1.
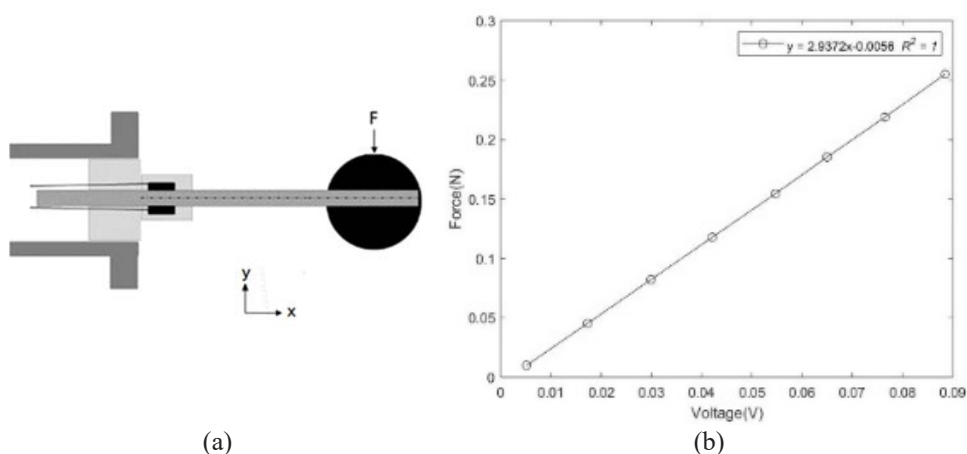

| (a) | (b) |

Figure 1: Measurement system. (a) Schematic representation; and (b) Calibration chart.

3 VALIDATION METHODS, MEASUREMENTS AND RESULTS

For validation purposes, the sensor was initially tested with a confined flow inside a tube and later effects of an impinging jet were studied. Finally, the sensor used to measure force from particle flows with different conditions; with varying impact height, size and density of the particles.

3.1 Aerodynamic drag acting on a sphere

A stationary object immersed in a fluid flow experiences a drag force from the flow, which varies with fluid velocity and properties as well as the object characteristics, such as shape and size. For this study, the sensor was immersed in an upward airflow in ambient conditions inside a tube with 11 cm in diameter and flow velocities up to 5 m/s. The force measured by the sensor consisted of the drag force exerted on the beam and the ball, and to separate these, the force measurements were conducted without the ball and subtracted from all the collected data. The drag force can be written as:

$$F_D = \tfrac{1}{2} C_D A \rho V^2, \tag{1}$$

where C_D is the drag coefficient, A the cross sectional area to the flow, ρ and V are the density and velocity of the fluid, respectively. The drag coefficient equations for a sphere are presented as an empirical relations to the Reynolds number of a particle, given as:

$$Re_s = \frac{\rho_f |v_s - v_f| d_p}{\mu_f}, \tag{2}$$

where ρ_f is the density of the surrounding fluid, v_s is the velocity of the solid, which in this case is equal to zero since the sensor is fixed, v_f is the superficial velocity of the fluid, d_p is the particle diameter and μ_f is the dynamic viscosity of the fluid. In the calculation, the air was considered as an ideal gas.

The measured forces are compared with theoretical drag forces calculated with three correlations for the drag coefficient:

- Clift et al. [8]:

$$C_D = \begin{cases} 24/Re_s + 3/16 & \text{for } Re_s < 0.01 \\ (24/Re_s)\left(1 + 0.1315Re_s^{0.82-0.05logRe}\right) & \text{for } 0.01 < Re_s \leq 20 \\ (24/Re_s)(1 + 0.1935Re_s^{0.6305}) & \text{for } 20 < Re_s \leq 260 \\ 10^{1.6435-1.1242\,log\,Re_s+0.1558\,log^2\,Re_s} & \\ \quad \text{for } 260 < Re_s \leq 1500 & \\ 10^{-2.4571+2.5558\,logRe_s-0.9295\,log^2\,Re_s+0.1049\,log^3\,Re_s} & \\ \quad \text{for } 1500 < Re_s \leq 1.2 \times 10^4 & \\ 10^{-1.9181+0.637\,logRe_s-0.0636\,log^2\,Re_s} & \\ \quad \text{for } 1.2 \times 10^4 < Re_s \leq 4.4 \times 10^4 & \\ 10^{-4.339+1.5809\,logRe_s-0.1546\,log^2\,Re_s} & \\ \quad \text{for } 4.4 \times 10^4 < Re_s \leq 3.38 \times 10^5 & \\ 29.78 - 5.3\,logRe_s & \text{for } 3.38 \times 10^5 < Re_s \leq 4 \times 10^5 \\ 0.1logRe_s - 0.49 & \text{for } 4 \times 10^5 < Re_s \leq 4 \times 10^6 \\ 0.19 - 8 \times 10^4/Re_s & \text{for } Re_s > 10^6 \end{cases} \tag{3}$$

- Schiller and Neumann [8]:

$$C_D = \begin{cases} \frac{24}{Re_s}(1 + 0.15 Re_s^{0.687}), \text{ for } Re_s < 1000 \\ 0.44, \text{ for } Re_s \geq 1000. \end{cases} \tag{4}$$

- Clift and Gauvin [9], [10]:

$$C_D = \frac{24}{Re_s}(1 + 0.15 Re_s^{0.687}) + \frac{0.42}{1 + 42500 Re^{-1.16}}. \tag{5}$$

The results of the measured and theoretical drag forces are presented in Fig. 2. The Mean Square Error varies from 12.67% to 28.5% between the three evaluated cases. The initial calibration can affect the values and to reduce the inaccuracy of the measurement, a frequently calibration of the system is made during the samples time between experiments.
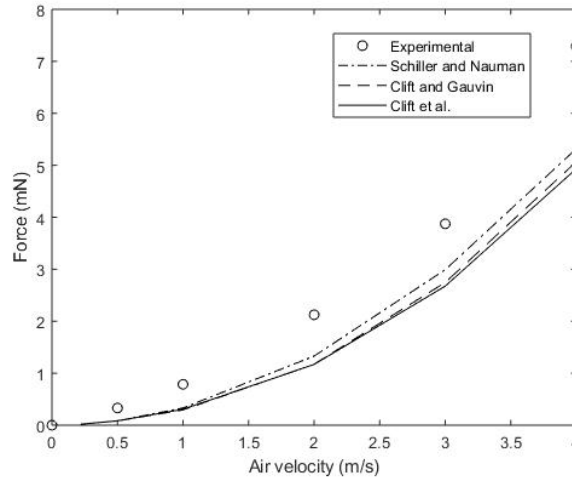

Figure 2: Drag force on a sphere immersed in an air flow.

3.2 Jet impingement on a sphere

To expand the measurements to another type of momentum transfer, impingement tests were performed with a water jet. A syringe with a nozzle diameter of 3.98 mm was used to produce a controlled water jet, with a weighted object pressing the piston with a constant force. Compared to particles, it is more straightforward to determine the momentum impacting the sensor, as the jet is continuous and the determination of the velocity is simpler. Normal tap water was used as the working fluid with a temperature of 20°C, viscosity of 0.001 Pa s and density of 998.2 kg/m^3. Each test was repeated 5 times for three different distances between the nozzle and the impingement surface, the data were processed according the description formulated in Section 2. The impingement test setup is described in Fig. 3.

As the distance in height between the nozzle and the surface of the sphere increases, the larger the forces obtained as the gravitational acceleration affects the jet. The force can also be controlled by changing the weight of the pressing object. The velocity of the water jet before the impact is calculated to estimate the force over the surface, which is expressed as:
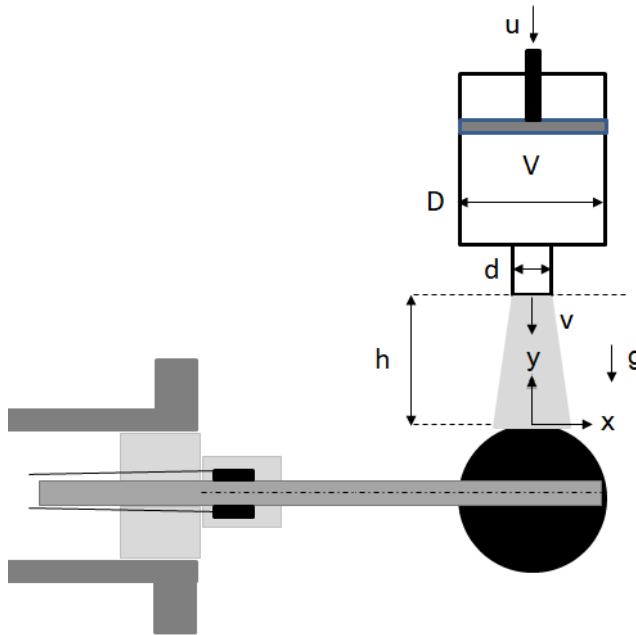
$$F = ma = \rho q_v v_i, \tag{6}$$

Figure 3: Water impinging jet.

where m is mass, a acceleration, ρ density of water, q_v is volumetric flow rate and v_i is velocity before the impact. Considering the water as an incompresible fluid, the volumetric flow rate remains constant throughout the syringe and the nozzle:

$$q_v = uA_1 = vA_2, \qquad (7)$$

where u represents the velocity of the piston, v is the velocity at the nozzle, A_1 and A_2 are the sectional area of syringe cylinder and the nozzle, respectively. The velocity of the piston was determined with a Phantom Miro M310 High Speed Camera with a frame rate of 100 fps. The information of the location of the piston over time was processed in MatLab using component analysis of the binary images. The velocity of the jet at the nozzle was then computed with eqn (7). The effect of gravity on the stream was acknowledged in computation of the velocity before the impact with the equations of motion:

$$v_i = v + gt, \qquad (8)$$

$$h = vt + 1/2\, gt^2, \qquad (9)$$

in which the distance between the nozzle and the surface of the sphere is h and g is the gravitational acceleraton.

To illustrate the experimental measures and the theoretical calculated trend, an example of results for an inpinging height of 1.5 cm are shown in Fig. 4, in which is visible that velocity and the force of the jet increase during the press, with both the theoretical and measured forces presenting the same slope but the theoretical values are on average 16% larger than the force measured by the sensor.

A comparision between experimental and theoretical forces excerted by the water jet for different heights is presented in Fig. 5.
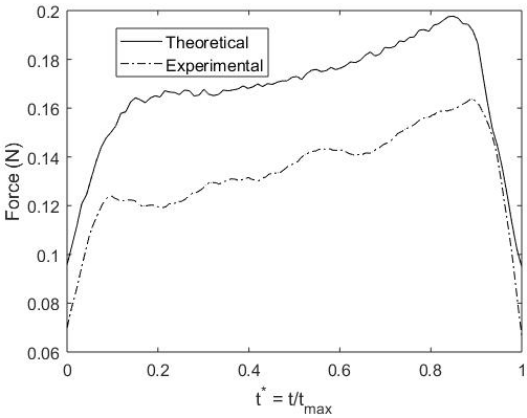
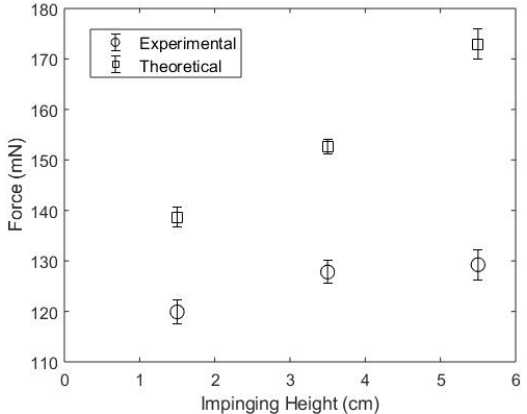Figure 4: Experimental and theoretical forces at 1.5 cm impinging height.

Figure 5: Experimental and theoretical forces of the impinging jet.

As seen from the results, there are clear differences between the theoretical, maximum force and the force measured with the sensor. The discrepancies between the theoretical and the experimental values increase with the height, reaching a 37.6% difference for the higher level. This is expected, as the momentum transfer from the jet to the sensor is limited. Initially, the jet hits the curved surface of the sensor, and due to the curvature, part of the momentum is redirected. After the initial impact, there remains a layer of water on top of the sensor and the incoming jet hits this layer, transferring parts of its momentum on the water layer rather than the sensor. Thus, the presented results should not be directly compared to the theoretical values, but rather they indicate the behaviour to be expected from the measurements. In this light, the obtained results are logical and reasonable.

3.3 Particle stream on a sphere

The sensor was used to measure the forces exerted on the sphere by a stream of falling particles with different properties. Unlike with the water jet, the momentum impacting the

sensor could not be determined as, unfortunately for the current research, the particle velocities or concentrations at the impact could not be measured. The effect of the falling height, the size and density of the particles were studied. The falling height relates to the impact velocity of the particles, as they are accelerated more by gravity with larger height. A total of 3 repetitions were done for each configuration, in order to have statistical representative values. The output signal was processed according to the description in Section 2. A constant mass of 300 g of particles was used for all the cases. The particles were fed through a funnel with a nozzle diameter of 3 cm and mesh grids of 2, 1 and 0.5 mm were placed at the nozzle of the funnel, sizes large enough to avoid the obstruction of the mesh, to distribute the particles. The list of materials used in the experiments are summarize in Table 1. A schematic visualization of the setup is shown in Fig. 6.

Table 1: Material properties description.

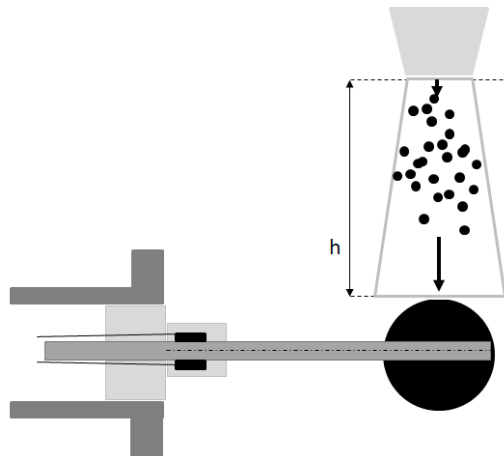| Material	Material density (kg/m^3)	Particle diameter (μm)	Falling height (cm)
Glass beads	2500	700–1000	2.2,4.2,6.2
		500–560	2.2
		180–250	2.2
Zirconium oxide	4135	180–250	2.2
Iron beads	7645	180–250	2.2

Figure 6: Schematic view of the particle–particle force measurement system.

As an example, the force measured using glass particles 500–560 μm released from a height of 2.2 cm from the surface is shown in Fig. 7, in which a relatively constant force can be observed.

The average forces for the different cases are presented in Fig. 8. The largest glass particles were used for testing the effect of different heights (impact velocities). As the distance from the surface increases, the impact velocities increase and higher forces are observed, as seen in Fig 8(a). The impact force is also a function of density of the particles,
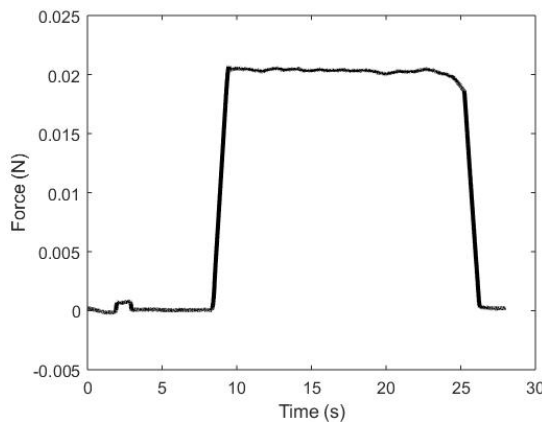
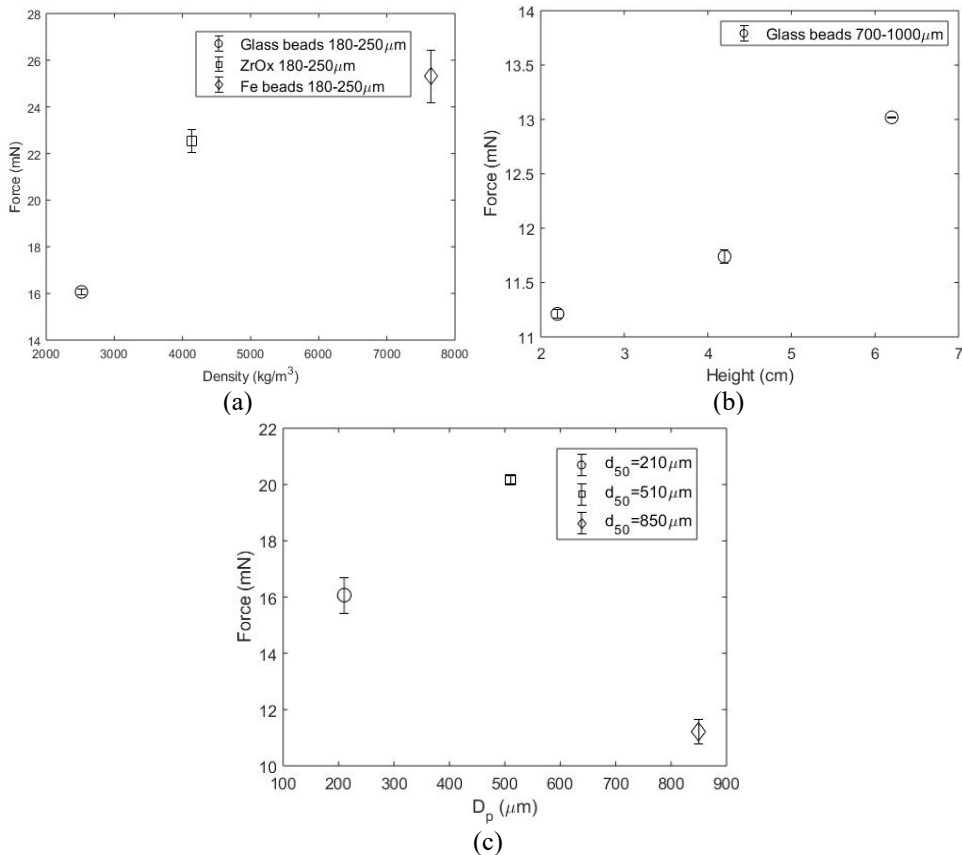Figure 7: Force from glass beads 500–560 µm from height of 2.2 cm.

(a)

(b)

(c)

Figure 8:   Measured impact forces with (a) Different heights for glass beads 700–1000 µm; (b) Different material densities; and (c) Different particle sizes.

and this was tested with glass beads, zirconium oxide and iron beads sieved to have the same particle size range. As the density of the particles increases, the resulting forces are larger as shown in Fig. 8(b). Similar analysis can be made for particles of different size, higher forces should be observed with larger particle size. This was investigated with glass bead particles of different size, with results presented in Fig. 8(c). While the forces for the small and middle size particles shown an ascendant trend, the measured forces for the large particles present a sudden drop. Unfortunately the particle velocities and concentrations could not be measured in this study, to confirm the reason for this behaviour. Most likely this is related with the particle distribution system, it is not feasible to have the same number of particle hitting the sensor with different materials, thus there were less particles large size impacting the sensor at a given time compared to the smaller particles. Additionally, a fixed mass of particles was used, which reduces the number of the larger particles compared to the smaller particles.

4 CONCLUSION

A force sensor using strain gages was developed in order to investigate momentum transfer from the particle phase in the fluidized beds. The sensor was tested in air flow to measure the gas–solid drag force on a single ball. In addition, momentum transfer to the ball was measured from a water jet and falling particle stream. These initial measurement results were reasonable which shows the reliability of the sensor and the measurement method. In future, the study will be continued by determining the velocities and concentration of particles before the impact with the object to better link the particle properties and flow conditions with the momentum transfer. Also, the setup will be used to measure particle collisional forces inside a laboratory scale fluidized bed reactor.

ACKNOWLEDGEMENT

REFERENCES

[1]   Gidaspow, D., Bezburuah, R. & Ding, J., Hydrodynamics of circulating fluidized beds: Kinetic theory approach. *Proceedings of the 7th Engineering Foundation Conference on Fluidization*, pp. 75–82, 1992.

[2]   Lun, C.K.K., Savage, S.B., Jeffrey, D.J. & Chepurniy, N., Kinetic theories for granular flow: Inelastic particles in Couette flow and slightly elastic particles in a general flow field. *Journal of Fluid Mechanics,* **140**, pp. 223–256, 1984.

[3]   Payman, J. & Hyppänen, T., Momentum transport between two granular phases of spherical particles with large size ratio: Two-fluid model versus discrete element method. *Powder Technology*, **273**, pp. 13–18, 2015.

[4]   Syamlal, M., The Particle–Particle Drag Term in a Multiparticle Model of Fluidization. Topical Report DOE/MC/21353--2373, 1987.

[5]   Bell, R.A., Numerical Modelling of Multi-Particle Flows in Bubbling Gas–Solid Fluidized Beds. PhD thesis, Swinburne University of Technology, 2000.

[6]   Hideyuki, T., Katsuhiro, I., Tomoyuki, K., Kazuo, S. & Syuichi, U., Design and evaluation of strain gauge force balance with short test duration. *Transactions of the Japan Society for Aeronautical and Space Sciences*, **48**(159), pp. 1–6, 2005.

[7]   Maruyama, T., Optimization of roughness parameters for staggered arrayed cubic blocks using experimental data. *J. Wind. Eng. Ind. Aerodyn.*, **46–47**, pp. 165–171, 1993.

[8]   Clift, R., Grace, J. & Weber, M., *Bubbles, Drops and Particles*, Dover Publications: New York, 2005.

[9]   Turton, R., & Levenspiel, O., A short note on the drag correlation for spheres. *Powder Technology*, **47**(1), pp. 83–86, 1986.

[10] Flemmer, R.L.C. & Banks, C.L., On the drag coefficient of a sphere. *Powder Technology*, **48**(3), pp. 217–221, 1986.